

Formation of Cavities, Filaments, and Clumps by the Non-linear Development of Thermal and Gravitational Instabilities in the Interstellar Medium under Stellar Feedback

Keiichi Wada¹, Marco Spaans², and Sungeun Kim³

¹*National Astronomical Observatory, Mitaka, 181-8588, Japan*

Email: wada.Keiichi@nao.ac.jp

²*Harvard-Smithsonian Center for Astrophysics, 60 Garden Street, Cambridge, MA 02138*

³*Astronomy Department, University of Illinois at Urbana-Champaign, Urbana, IL 61801*

ABSTRACT

Based on our high resolution, two-dimensional hydrodynamical simulations, we propose that large cavities may be formed by the nonlinear development of the combined thermal and gravitational instabilities, without need for stellar energy injection in a galaxy modeling the Large Magellanic Clouds (LMC). Our numerical model of the star formation allows us to follow the evolution of the blastwaves due to supernovae in the inhomogeneous, multi-phase, and turbulent-like media self-consistently. Formation of kpc-scale inhomogeneity, such as cavities, observed H I map of the LMC, is suppressed by frequent supernovae (average supernova rate for the whole disk is $\sim 0.001 \text{ yr}^{-1}$). However the supernova explosions are necessary for the hot component ($T_g > 10^{6-7} \text{ K}$). Position-velocity maps show that kpc-scale shells/arcs formed through the nonlinear evolution in a model without stellar energy feedback has similar kinematics to explosive phenomena, such as supernovae. We also find that dense clumps and filamentary structure are formed due to a natural consequence of the non-linear evolution of the multi-phase ISM. Although the ISM in a small scale looks turbulent-like and transient, the global structure of the ISM is quasi-stable. In the quasi-stable phase, the volume filling factor of the hot, warm, cold components are ~ 0.2 , ~ 0.6 , and ~ 0.2 , respectively. We compare the observations of H I and molecular gas of the LMC with the numerically obtained H I and CO brightness temperature distribution. The morphology and statistical properties of the numerical H I and CO maps are discussed. We find that the cloud mass spectrum of our models represent a power-law shape, but their slopes change between models with and without the stellar energy injection, and also the slope depends on the threshold brightness temperature of CO.

Subject headings: ISM: structure, kinematics and dynamics — galaxies: structure — individual: LMC — method: numerical

1. INTRODUCTION

The topology of the neutral interstellar medium (ISM) can be studied in great detail by the spatial and velocity structures in the neutral H I gas. A recent high-resolution H I survey of the Large Magellanic Cloud (LMC) reveals that the structure of the neutral atomic inter stellar gas is dominated by numerous holes and shells as well as complex filamentary structure (Kim et al. 1998). These features are commonly seen in recent high-resolution H I images of nearby galaxies obtained with radio synthesis interferometers (Deul & den Hartog 1990; Puche et al. 1992; Staveley-Smith et al. 1997; Walter & Brinks 1999; Stanimirovic et al. 1999). In general, the shell-like and hole structure seen in H I has been understood as the cumulative effect of stellar winds from massive stars and supernova explosions evacuating the cool ISM (Tenorio-Tagle 1988; van der Hulst 1996; Oey 1996 ; Oey & Clarke 1997). However, the extensive study of H I shells in the LMC shows that there is a relatively weak correlation between the H I shells and the ionized gas traced out by the H II regions and H II filaments (Kim et al. 1999). Furthermore, the correlation between the H I shells and 122 OB stellar associations in the LMC is not very tight (Kim & Chu 2000). Rhode et al. (1999) claimed that there is no remnant star clusters at the center of the H I holes in Holmberg II, and it is inconsistent with the SNe hypothesis. Moreover an energy source generating the kpc-scale supergiant H I holes is a puzzle. These issues raise an interesting question about whether H I shells/holes have been formed by the interaction between stars and the ISM or not.

Recent hydrodynamical simulations by Wada & Norman (1999) demonstrate that a gravitationally and thermally unstable disk, which models an ISM in galaxies, can generate the cold, dense clumps and filaments surrounded by hot, diffuse medium. They show that porous structure is a natural consequence of the non-linear evolution of the ISM. This result strongly suggests that some fraction of H I shells, supershells or holes seen in galaxies does not relate to the interaction between stellar activities and the ISM.

The other important component of the ISM is the molecular gas. Molecular clouds are potential sites of star formation, but their formation mechanism, and the relationship between their evolution and star formation have been poorly understood. Dense molecular hydrogen is traced by the rotational transition

of CO, and a recent high resolution survey of ^{12}CO ($J=1-0$) in the LMC with NANTEN, which is 4m millimeter-wave telescope at Las Campanas Observatory, established a comprehensive view of the giant molecular clouds in the LMC (Fukui et al. 1999). Since the gas clumps, whose size is typically 10 – 100 pc, in the simulations by Wada & Norman (1999) are dense ($n > 1000 \text{ cm}^{-3}$) and cold ($T = 10 - 100 \text{ K}$), they are counterparts of the observed giant molecular clouds in the LMC or other galaxies.

Using numerical simulations, Feitzinger et al. (1981) and Gardiner, Turfus, & Putman (1998) have studied global dynamics of the ISM and star formation in the LMC. Although the numerical methods they used are different, the stochastic self-propagating star formation model (e.g. Seiden & Gerola 1984) in Feitzinger et al. (1981) and sticky particle method in Gardiner, Turfus, & Putman (1998), are both phenomenological concerning the structure and dynamics of the ISM and star formation processes. Unfortunately the spatial resolution (100 pc in Feitzinger et al. 1981) and mass resolution ($6 \times 10^4 M_{\odot}$, which corresponds to $\sim 200 \text{ pc}$ for $n \sim 1 \text{ cm}^{-3}$ and $H \sim 100 \text{ pc}$, in Gardiner, Turfus, & Putman 1998) in these simulations are not good enough for comparison between models and the recent high resolution observations ($\sim 15 \text{ pc}$ for HI (Kim et al. 1998) and $\sim 40 \text{ pc}$ for CO ($J=1-0$) (Fukui et al. 1999)).

In this paper, we apply the numerical scheme used in Wada & Norman (1999) to a LMC-type model galaxy, and we conduct two-dimensional hydrodynamical simulations of the multi-phase ISM in a LMC-like model galaxy, taking into account self-gravity of the gas, radiative cooling and various heating processes, such as supernova explosions. High spatial resolution (7.8 pc) and a modern hydrodynamical scheme allow us to model the star formation and its feedback less phenomenologically, and therefore it needs less assumptions than the previous semi-analytic and numerical approaches (e.g. a review by Shore & Ferrini 1995). In contrast to the model used in Wada & Norman (1999), the rotation curve assumed here is nearly rigid as suggested in the LMC or other LMC-type dwarf galaxies. We derive the H I and CO brightness map from the simulations. Then we compare these simulation results with the H I and CO observations of the LMC.

In §2, we describe our numerical method and models. In §3, the numerical results with and without star formation are discussed on morphology and statisti-

cal structure of the ISM, then they are compared with the observations. Position-Velocity diagrams derived from the numerical results are also discussed. Comparison with past numerical simulations and other implications are discussed in §4, and conclusions are presented in §5.

2. NUMERICAL METHOD AND MODELS

Taking into account the multi-phase and inhomogenous nature of the ISM is crucial for realistic simulations of global star formation in galaxies. Stars are formed preferentially in cold molecular gas, and supernovae produce low density, high temperature gas. Interaction between such different phases are also important (e.g. McKee & Ostriker 1977; Ikeuchi, Habe, & Tanaka 1984). In order to simulate dynamics of the inhomogeneous, multi-phase interstellar matter and star formation, our numerical method has following features. (1) High spatial resolution (7.8 pc), for diffuse gas to high density gas. We use an Euler mesh code with 1024^2 Cartesian grid points. (2) The simulations are global in order to study effects of galactic rotation and other kpc scale phenomena to the local structure of the ISM. (3) Self-gravity of the gas is calculated. (4) Radiative cooling for gas whose temperature is between 10^8 K and 10 K is taken into account. (5) Various heating processes are included. Here we assume photoelectric heating due to dust grains and UV radiation, SN explosions, and stellar wind from massive stars. (6) High numerical accuracy for shocks is achieved with a modern hydrodynamical scheme. This is crucial, because the ISM is usually supersonic, and SNe produce strong shocks.

We solve the following hydrodynamical equations and the Poisson equation numerically in two dimensions to simulate the evolution of a rotating gas disk in a stellar potential.

$$\frac{\partial \rho}{\partial t} + \nabla \cdot (\rho \mathbf{v}) = 0, \quad (1)$$

$$\frac{\partial \mathbf{v}}{\partial t} + (\mathbf{v} \cdot \nabla) \mathbf{v} + \frac{\nabla p}{\rho} + \nabla \Phi_{\text{ext}} + \nabla \Phi_{\text{sg}} = 0, \quad (2)$$

$$\frac{\partial E}{\partial t} + \frac{1}{\rho} \nabla \cdot [(\rho E + p) \mathbf{v}] = \Gamma_{\text{UV}} + \Gamma_{\star} - \rho \Lambda(T_g), \quad (3)$$

$$\nabla^2 \Phi_{\text{sg}} = 4\pi G \rho, \quad (4)$$

where, ρ, p, \mathbf{v} are the density, pressure, and velocity of the gas, and the specific total energy $E \equiv |\mathbf{v}|^2/2 + p/(\gamma - 1)\rho$, with $\gamma = 1.4$. We assume a time-independent external potential $\Phi_{\text{ext}} \propto v_c^2/(R^2 + a^2)^{1/2}$, where $a = 2.5$ kpc is a core radius of the potential and $v_c = 63$ km s $^{-1}$ is the maximum rotational velocity, and they are determined to mimic the rotation curve of the LMC (Kim et al. 1998). Since the total gas mass is about 10 % of the total dynamical mass (see below), the effect of self-gravity of the gas to the rotation curve is not significant. In fact the rotation curve after the system evolves is close to the rigid rotation (see §3.3 and the position-velocity diagrams in Fig. 10).

We also assume a cooling function $\Lambda(T_g)$ ($10 < T_g < 10^8$ K) (Spaans & Norman 1997). The cooling processes taken into account are, (1) recombination of H, He, C, O, N, Si and Fe, (2) collisional excitation of HI, CI-IV and OI-IV, (3) hydrogen and helium bremsstrahlung, (4) vibrational and rotational excitation of H₂ and (5) atomic and molecular cooling due to fine-structure emission of C, C⁺ and O, and rotational line emission of CO and H₂. As a heating source, Γ_{UV} , we assume a uniform UV radiation field (Gerritsen & Icke 1997), which is normalized to the local interstellar value, and photoelectric heating by grains and PAHs. The bulk of the heating for the $10^2 - 10^4$ K gas is provided by photo-emission of UV irradiated dust grains (Bakes & Tielens 1994).

We consider two feedback effects of massive stars on the gas dynamics, namely stellar winds and supernova explosions, although our results show that the former is less effective than the latter. We first identify cells which satisfy criteria for star formation. The criteria are a surface density threshold $(\Sigma_g)_{i,j} > \Sigma_c$ and a critical temperature $(T_g)_{i,j} < T_c$ below which star formation is allowed. The surface density is defined as $\Sigma_g = 2H\rho$, where H is the scale height and assumed to be constant (100 pc). In these simulations we take $\Sigma_c = 40M_{\odot} \text{ pc}^{-2}$ and $T_c = 15$ K (model ‘Star Formation 1’, hereafter ‘SF1’) and ten times larger threshold density, $\Sigma_c = 400M_{\odot} \text{ pc}^{-2}$ and $T_c = 15$ K (model SF2). These criteria are chosen to satisfy the condition, $L_J < 0.1\Delta$ or $L_J < 0.01\Delta$, where L_J and Δ are the Jeans length and the size of each cell. The volume filling factors of the star-forming cells to the total volume are typically $\sim 5 \times 10^{-3}$ and $\sim 5 \times 10^{-4}$ for model SF1 and SF2, respectively. Namely the star forming sites are cold, clumpy regions. We also assume the star-forming criteria must

last during 10^5 yr for each cell before the star formation is initiated. Since the spatial resolution is fine enough compared to the GMC size, we do not have to assume any global criteria for gravitational instability to identify star forming sites. Assuming the Salpeter IMF with $m_u = 120M_\odot$ and $m_l = 0.2M_\odot$, we create test particles representing massive stars ($\geq 8M_\odot$) in the star forming cell. The kinematics of the test particles in the external potential and the self-gravity potential of the gas are traced by the second-order time-integration method. The stars (test particles) inject energy due to stellar winds during their lifetime which is approximately $\sim 10^7$ yr (Leitherer, Robert, & Drissen 1992). When one of stars represented by a test particle explodes as supernova, an energy of 10^{51} ergs is injected into the cell as thermal energy where the test particle is located at that moment. The cooling procedure is not used for such cells, but the cells adjoining the supernova cell are treated normally. Evolution of the supernova remnant is very dependent on its environment. In contrast to past numerical studies of the ISM with supernova explosions on a galaxy scale, we do not introduce simple evolutionary models for the SNR, such as the Sedov solution, and heating efficiency for the ISM due to a supernova. With our code, two-dimensional evolution of blast waves caused by supernovae in an inhomogeneous and turbulent medium with global rotation is simulated explicitly. Therefore, we can trace consistently the thermal and dynamical evolution of the ISM around the star forming regions and the associated supernovae remnants and superbubbles (c.f. Norman & Ikeuchi 1989)

The hydrodynamic part of the basic equations is solved by the third-order AUSM (Advection Upstream Splitting Method) (Liou & Steffen 1993). After testing this code for various hydrodynamical 1-D and 2-D problems, we find that AUSM is as powerful a scheme for astrophysical problems as are the PPM (Woodward & Colella 1984) and Zeus (Stone & Norman 1992) codes. More details about our numerical code and test results are described in Wada & Norman (2000, in preparation).

We use 1024^2 Cartesian grid points covering a $8\text{ kpc} \times 8\text{ kpc}$ region. The spatial resolution is 7.8 pc . A periodic Green function is used to calculate the self-gravity for the $8\text{ kpc} \times 8\text{ kpc}$ region with 2048^2 grid points (Hockney & Eastwood 1981). The second-order leap-frog method is used for the time integration. We adopt implicit time integration for

the cooling term in equation (3).

The initial disk is an axisymmetric and rotationally supported ($R = 3.7\text{ kpc}$) with uniform surface density, $\Sigma_g = 12M_\odot\text{ pc}^{-2}$, and the total gas mass is $5 \times 10^8 M_\odot$ (Kim et al. 1998). Random density and temperature fluctuations are added to the initial disk. Amplitude of the initial fluctuations is less than 5 % of the unperturbed values and have an approximately white noise distribution. The initial temperature is set to 10^4 K ($R \leq 3.7\text{ kpc}$) and 10^2 K ($R > 3.7\text{ kpc}$). The reason why we chose the low temperature in the outer region is to avoid the numerical artifact of the boundaries, i.e. reflection and generation of waves or shocks, for the initial evolution of the gas disk. In ghost zones at the boundaries of the calculating region (i.e. $8 \times 8\text{ kpc}^2$), all physical quantities remain at their initial values during the calculations. From test runs we found that this boundary condition is much better than ‘outflow’ boundaries, because the latter cause strong unphysical reflection of waves at the boundaries.

3. RESULTS

3.1. Evolution and Structure of the ISM

3.1.1. Model without Star Formation

Figure 1 shows the time evolution of density and temperature of a model without star formation and its feedback (hereafter we call this model ‘model NSF’). Due to gravitational and thermal instability in the gas disk, clumpy fluctuations evolve in the first 10^8 yr, and then the clumps merge and form larger structure. They are deformed by the local tidal field and global shear in the non-linear phase, and as a result, filamentary structure is formed. Higher density clumps ($\Sigma_g > 10^3 M_\odot\text{ pc}^{-2}$) are formed in the filaments due to the gravitational instability, or collisions between the filaments. The high temperature cavities ($T > 10^5\text{ K}$) are formed due to shock heating. The dynamical time scale for the large ($L \sim 200\text{ pc}$) high temperature ($T \sim 10^5\text{ K}$) region seen in the temperature panel at $t = 800\text{ Myr}$ is $\tau_{\text{dyn}} \sim L/\Delta v \sim 200\text{ pc}/20\text{ km s}^{-1} \sim 10^7\text{ yr}$. The cooling time, τ_{cool} on the other hand, for this low density region ($n \sim 10^{-3}$) is $\sim 2 \times 10^7\text{ yr}$ (Spitzer 1977), which is comparable to τ_{dyn} . In fact the high temperature cavity is a tentative structure that lasts $\sim 10^7\text{ yr}$. Photo-electric heating and UV irradiation contribute to form $T \sim 10^4\text{ K}$ gas. In the high density ($\Sigma_g > 10^2 M_\odot\text{ pc}^{-2}$) fila-

ments and clouds, the temperature is less than 100 K because the radiative cooling is effective. The global structure of the disk does not change significantly after 400 Myr, and it reaches a quasi-steady state. Figure 2 is time evolution of the volume filling factor, f_v , of each temperature level and time evolution of the maximum density. This also represents that the global ($>$ kpc scale) system reaches a quasi-stationary state after $t \sim 300$ Myr. This period is comparable to the local free fall time t_{ff} for the initial density, $t_{ff} \sim 200(\Sigma_g/12M_\odot \text{ pc}^{-2})^{-1/2}$ Myr. At the global quasi-steady state, the warm gases ($T_g = 100 - 10^4$ K) occupy a large volume ($\sim 60\%$ of the whole calculating region), and $f_v \sim 20\%$ for the cold ($T_g < 100$ K) and $f_v \sim 20\%$ for hot gas ($T_g = 10^4 - 10^5$ K). The maximum density in the same plot show slower evolution after $t \sim 300$ Myr than the non-linear evolutional phase.

One should note, however, that the globally stable state does not mean the local filamentary and porous structure whose scale is less than 1 kpc. It is rather quite dynamic and transient, which is similar to the past turbulent ISM models (Bania & Lyon 1980; Chiang & Prendergast 1985; Chiang & Bregman 1988; Rosen & Bregman 1995; Vázquez-Semadeni et al. 1995; Passot, Vázquez-Semadeni, & Pouquet 1995; Gazol & Passot 1999). Clump mass is increasing during the initial linear and non-linear evolutional phase ($t < 200$ Myr) due to the mass accretion and merging with other clumps or filaments, but in the quasi-stationary phase, disruption processes of the clumps, such as local tidal field (e.g. interaction between clumps, or shear) or shocks, prevent monotonic increase of the mass of each clump. Since we introduce the cutoff temperature for the cooling (i.e. 10 K), the gaseous pressure prevent the dense clouds further collapsing towards singularities. The angular momentum also supports the clouds (see §3.3).

The density and temperature structures (Fig. 1) are similar to those in the model of Wada & Norman (1999), where a smaller disk is investigated (the radius is 1 kpc), but the present model shows kpc-scale inhomogeneity and a more asymmetric distribution against the galactic center. This difference is probably caused by the difference of the rotation curves used in the two models: a rigid rotation or differential rotation. With a rigid rotation, random and turbulent motion dominates the circular rotation in the central region. With the global shear, on the other hand, global spirals develop toward the galactic cen-

ter.

3.1.2. Models with Star Formation

Figure 3 represents density and temperature maps of the model SF2 at $t = 833$ Myr. The model SF1, which has ten times smaller threshold density for the star formation criterion (see §2), shows very similar density morphology and temperature structure. The red regions in the temperature map are hot gaseous regions where $T_g > 10^6$ K. They are young ($< 10^6$ yr) supernova remnants. Figure 3 also shows that most young supernova remnants are not axisymmetric. This is caused by that the background ISM is highly inhomogeneous, and the radiative cooling at the dense filaments is so effective, and that it prevents the blastwaves expanding axi-symmetrically. Typical size of the hot cavities is less than 500 pc. Some bubbles together form kpc scale ‘super bubbles’. The hot region around $(-3, -1)$ is one of the examples. Note that the size of the cavities is expected to change away from the galactic plane in a 3-D model (see also §4).

Although the filamentary and clumpy structures of the gas which result in the star forming models are similar to those of model NSF, the kpc scale inhomogeneity seen in the the model (Fig. 1) is not apparent in the SF models. The large scale inhomogeneity in the model SF1 and SF2 is less prominent than that of the model NSF. This is because that the time scale for making the kpc-scale holes, which is a dynamical time scale, $\sim 10^8$ yr, is much longer than the the time scale for supernova explosions and evolution of the blastwaves, $\lesssim 10^6$ yr. Approximately 10^3 supernovae per kpc^2 explode in this model during $\sim 10^8$ yr. The kpc-scale low density cavities, which is formed due to evacuation of gas by the effect of the gravitational and thermal instabilities, cannot evolve under such frequent supernova explosions.

We find that the supernova rate is fluctuate in a time scale $\sim 10^7$ yr, but it stays in a range $4-10 \times 10^{-4} \text{ yr}^{-1}$ during 6×10^8 yr in model SF2 (Fig. 4). This behavior also appears in model SF1, but the SN rate becomes smaller for the larger threshold density ($\sim 8-12 \times 10^{-4} \text{ yr}^{-1}$). ROSAT observed 46 supernova remnants and more candidates in the LMC (Haberl & Pietsch 1999). If we assume the ages of SNRs are between ~ 10000 yrs and ~ 30000 yrs, then we have SN explosion every 250 yrs or 750 yrs. This indicates about 0.0013/yr or 0.004/yr for SN rate in the LMC. If we use the larger threshold density for the

star formation in our model than that in model SF2, this results in smaller supernova rate than $\sim 0.001 \text{ yr}^{-1}$. Therefore the threshold density much larger than $400 M_{\odot} \text{ pc}^{-2}$ would be excluded for modeling the LMC, if we assume that the star formation efficiency is 10 % or less and the standard IMF.

In Figure 5, the star particles at $t = 245 \text{ Myr}$ in model SF1 are plotted, and one may compare it to the density distribution (the right panel) of the same snapshot. Massive stars are not uniformly distributed, but they form clusters ('OB associations'). It is notable that the distribution of the star clusters does not necessarily correlate to the inhomogenous gaseous structure. In other words, cavities are not necessarily associate with the 'OB associations'. This is also seen in simulations by other groups, for example 2-D simulations of a highly compressible isobaric, non-selfgravitational fluid with star formation (Scalo & Chappell 1999).

3.2. Line Emission Maps and Comparison with the Observations

With the numerical simulations, we have density, temperature, and velocity fields (spatial resolution: 7.8 pc). Using this information as an input, we compute H I 21 cm brightness map and CO (J=1-0) line map for model NSF and SF1 and SF2. These maps can be directly compared with the recent high resolution surveys of the LMC: H I with ATCA (Kim et al. 1998) and CO (J=1-0) with NANTEN (Fukui et al. 1999).

With the numerical results described above, the following procedure is followed to compute a H I 21 cm brightness map. It is assumed that atomic hydrogen is in mostly neutral form in those regions where the temperature is at least a factor of 2 less than 8000 K, a value typical of (mostly ionized) HII regions, and motivated by measurements of the kinetic temperatures of HI clouds and HI intercloud gas. It is also assumed that the H I level populations of interest follow a thermal distribution in those regions along the line of sight, and that this mostly neutral gas dominates the integrated emissivity. The line of sight is face-on, i.e., perpendicular to the grid used for the hydrodynamic simulations. The two-dimensional density indeed is used as a column density in the radiative transfer calculations. The latter are done in three dimensions by assuming a scale height for the neutral gas of $H=100 \text{ pc}$, thus converting the column density in a (constant) local density for each point along the

line of sight. It is this three-dimensional grid, with two-dimensional hydrodynamic information, that is used to determine the H I central brightness temperature in the Monte Carlo procedure (Spaans 1996), where the ambient radiation field and its interactions with matter is represented by a discrete number of "photon packages". This method is three-dimensional and explicitly includes optical depth effects as well as the detailed velocity field of the hydrodynamical simulations for photons that travel along lines of sight that are not face-on. These latter photon trajectories need to be incorporated when the level populations are not in thermal equilibrium, i.e., for CO. A local velocity dispersion ΔV of $1.29 \times 10^4 T^{1/2} \text{ cm s}^{-1}$ is adopted for a kinetic temperature T , with a minimum of 0.5 km s^{-1} due to micro turbulent motions. For each grid point in the hydrodynamical simulation, the Monte Carlo radiative transfer then yields the integrated H I 21 cm intensity along the line of sight.

For the CO (J=1-0) line, the approach is similar to the H I case, with the appropriate correction factor in ΔV for the different atomic weight of the CO molecule. Furthermore, a carbon chemistry is added to compute the abundance of CO (Spaans & Van Dishoeck 1997), for a dust abundance equal to 1/5 of Solar. This chemistry is well understood (van Dishoeck & Black 1988), and care has been taken to include, for each computed line of sight and corresponding column density, the important self-shielding transitions of H₂ and CO (c.f. Spaans et al. 1994). The ambient average interstellar radiation field, required for the ambient chemical balance, is determined by scaling with the LMC B band surface brightness in mag per square arcsecond with respect to Galactic. This typically yields an enhancement of a factor of 3 – 5 in the mean LMC energy density compared to Galactic. It is assumed, because the hydrodynamical simulations are two-dimensional, that, to compute the local CO emissivity and the ambient chemical equilibrium, the gas density is given by the particular line of sight column density divided by a scale height of $H = 100 \text{ pc}$ for the neutral gas. The latter number H does not strongly influence the qualitative features in the presented maps.

Figure 6 presents H I 21 cm and CO (J=1-0) line brightness temperature maps calculated from the numerical data of the NSF model at $t = 800 \text{ Myr}$, using the procedure described above. Figure 7 is the same plot as Fig. 6, but for model SF2 at $t = 834 \text{ Myr}$.

Size of the H I filaments, shells, and holes in model NSF is ~ 1 kpc. The filaments and cavities in the outer region ($R > 2$ kpc) of model SF2 are also kpc-scale. We would like to emphasize that large cavities (> 1 kpc) and filaments in model NSF are NOT caused by a direct dynamical effect of star forming activities, but by the non-linear development of gravitational and thermal instabilities.

The CO emission is localized in many clumps (size $\sim 10\text{--}100$ pc) or clouds complexes (size $\sim 0.1\text{--}1$ kpc) in model NSF. Such CO “cloud” complexes could be sites for active star forming regions, such as the 30 Dor star forming region in the LMC. Model SF2 shows more uniform distribution of “stars” than in model NSF.

Figure 8 (a) and (b) are mass spectra of *molecular clouds* obtained from the CO brightness temperature (T_B) distribution of models NSF and SF2. We identify *clouds* and their mass by the following procedure. Assuming a threshold T_B for the CO map (Figs. 6 and 7), then we have many *islands* of CO emission. Most *islands* are not round in shape, but elongated or filament-like shape. We derive the mass of the *islands* using the surface density of the simulation data. Therefore the mass in Fig. 8 is the total gas mass of each *island*, not the virial mass. Here we plot three histograms for three different thresholds. The mass spectra shows a power-law, which is roughly $dN_c/dM_c \propto M_c^{-1.7}$ for model NSF, where dN_c is number of clouds between the mass M_c and $M_c + dM_c$, but this slope does not significantly depend on the threshold brightness. On the other hand, the spectrum of the star forming model steeper than the model without the energy feedback especially for small threshold: $dN_c/dM_c \propto M_c^{-1.7}$, $M_c^{-2.3}$, and $M_c^{-2.7}$ for model SF2 with $T_B = 100$, 50, and 30 K, respectively. The behavior of the slope to the threshold T_B in the model NSF and SF2 means that the stellar energy feedback changes structure of low density envelope of the dense clumps.

The NANTEN survey discovered about hundred molecular clouds in the LMC, and the mass spectrum of them is $dN/dM_{\text{vir}} \propto M_{\text{vir}}^{-1.5 \pm 0.1}$ for a range between $10^{5\text{--}6} M_{\odot}$ (Fukui et al. 1999), where M_{vir} is the virial mass of the cloud estimated by using the observed line width. In our model, smaller clouds ($M_c < 10^5 M_{\odot}$) tend to have smaller mass compared to their virial mass estimated from their internal velocity dispersions. In other words, the smaller clouds are not in equilibrium, but rather in a transient phase (Vázquez-

Semadeni et al. 1995). We find a rather weak but positive correlation between the cloud mass M_c and the virial mass $M_{\text{vir}}^{1/2}$ in our model. The mass spectrum of the model SF2 would be $dN_c/dM_{\text{vir}} \propto M_{\text{vir}}^{-1.4}$, if we use the lowest threshold $T_B = 30$ K. A similar discussion for the interpretation of the cloud mass spectra based on two-dimensional numerical simulations of the interstellar medium has been given by Vázquez-Semadeni et al. (1997) (see §4).

The maximal mass of the clouds is approximately $10^{6.5} M_{\odot}$ and $10^{5.5\text{--}6} M_{\odot}$ in models NSF and models with the star formation (SF1 and SF2). This implies that very massive clouds ($> 10^6 M_{\odot}$) are difficult to grow under the frequent supernova explosions. The maximal masses of the observed molecular clouds are about $10^{6.5} M_{\odot}$ (Fukui et al. 1999), which seems to prefer the model NSF. However, this does not mean that the star formation and its energy feedback are not important for shaping the ISM in the LMC, but it implies that the largest clouds could evolve in preferentially an environment where SNe are not frequent. Though one should be careful to make comparison between the observed and numerical mass spectrum, because the definition and identification of the “cloud” is not exactly identical, and it is related to noise level in observations.

We also find that the H I map of the computational model shows similar statistical properties to the observed H I map. Figure 9 shows the H I luminosity function, i.e. the histogram of the observed and numerical H I map of the LMC. The H I brightness temperature has been computed from $T_B = S_{\nu} \lambda^2 / 2k_B \Omega_{sb}$. S_{ν} is the H I flux density, k_B is the Boltzmann constant, and Ω_{sb} is the solid angle of the synthesized beam of ATCA mosaiced map. The H I intensity is determined from the integral of the brightness temperatures $\int T_B dv$ over the peak H I line profile, where dv is the channel width in kilometers per second. The H I luminosity functions appear to be log-normal like distribution for both observed and model NSF. The distributions of the H I luminosity function of the model NSF and SF2 for lower surface brightness ($T_B < 1000$ K) are similar to the observed one. The model SF2, on the other hand, shows excess above $T_B > 1000$ K than the observations. These high brightness regions are originated from shock compressed, dense gas.

3.3. Position-Velocity Diagrams

Position-Velocity (PV) diagrams give us information on the kinematics of the ISM. In Fig. 10 (a), we show the PV diagram, in which y -component of velocity (v_y) is integrated through x -positions, for the gas $\Sigma_g < 10^2 M_\odot \text{ pc}^{-2}$ in model NSF. Many arc-like structures in Fig. 10 (a) look like expanding shells originating from explosive phenomena in the ISM. However, they are NOT caused by explosions because there is no energy input due to supernovae in model NSF. The arcs in the PV diagram are actually caused by the gases that form filament-like structure seen in the density map (Fig. 1). The filaments and shells exhibit non-circular motion of the order of 10 km s^{-1} , and their shape continuously changed. Here we would like to emphasize that, it is hard to distinguish, on the PV diagrams, between expanding shells and such shell-like structures which are changing in shape due to local random motion.

From Fig. 10 (b), which is the same as Fig. 10(a), but for $\Sigma_g > 10^2 M_\odot \text{ pc}^{-2}$, we find that the dense and compact clumps, rotating with $\sim 10 - 30 \text{ km s}^{-1}$, which are recognized as steep ‘dotted lines’ on the PV-diagram. Here we can identify about 80 clumps, and about half of them show retrograde rotation against the sense of galactic rotation. A representative one can be seen at $(x, v_y) = (-0.5, -50)$ and less prominent one is at $(1.5, 25)$ and $(3, 75)$. Rotation of the clouds is important for the internal structure, motion, and star formation in the molecular clouds. Unfortunately, the spatial resolution in the NANTEN survey ($\sim 40 \text{ pc}$) is insufficient to resolve the rotation of each molecular clouds of the LMC. High resolution observations and statistical analysis of kinematics of molecular clouds in external galaxies are necessary to understand the formation of molecular clouds and star formation processes.

Figure 10 (c) shows the similar features shown in Fig. 10 (a), but for model SF1 at $t = 610 \text{ Myr}$. Arc-like structures seen in the PV map for the NSF are not clearly shown in this map. This means that the line-of-sight velocity field is much more random and chaotic than the NSF model, and there is no prominent large-scale coherent motion in the ISM of the model with stellar energy feedback.

4. DISCUSSION

The comparison of our model calculations with the observations of the LMC indicates that the star for-

mation models are more consistent with the formation of small ($\ll \text{kpc}$) and hot bubbles ($T_g > 10^7 \text{ K}$), which have been detected by X-ray diffuse emission. The power law slope of cloud mass spectrum of the models is close to that of observed one. On the other hand, the model calculations without the stellar feedback show even better agreement with global inhomogeneity of the HI and CO gas in the LMC, and also the HI distribution function is well represented in the model NSF. Therefore, it is most likely that energy feedback to the ISM from massive stars and supernovae explosions are important processes for producing hot gas, but they do not necessarily dominate dynamics and formation processes for the large scale inhomogeneity observed in HI and CO gas in the LMC. However, one should note that the initial condition of the models (i.e. axisymmetric and uniform density distributions) causes nearly uniform star formations in the whole disk. If we begin the simulations from a more inhomogeneous disk, stars will be formed non-uniformly, and effects of the stellar feedback are different, depending on location of the disk. We suspect that the more realistic model of the ISM in the LMC-type galaxy would be between our two extreme cases, but that can not be achieved by changing the threshold density of the star forming model.

In our models with stellar feedback, typical sizes of the hot cavities are less than 500 pc. Some ‘superbubbles’ can be formed in a outer disk region, and their linear sizes are $\sim \text{kpc}$ (see Fig. 3). Rosen & Bregman (1995) revealed in their two-dimensional, two-fluid (stars and gas) simulations in a disk galaxy that hot bubbles are formed by stellar activities, and their sizes depend on the energy injection rate. In their simulations, the linear size of the bubbles is up to $\sim 500 - 1000 \text{ pc}$ for the supernova rate is $0.0075 - 0.03 \text{ yr}^{-1}$. This rate is 1-2 orders of magnitude larger than that of our star forming models. Local, three dimensional MHD simulations of the ISM with supernova explosions by Korpi et al. (1999) show that the linear size of the superbubbles are typically 200-400 pc, which is consistent with our SF models. Gazol-Patino & Passot (1999) compute the evolution of the ISM in a region of the Galactic plane of size 1 kpc^2 in two-dimensional periodic domain. They found that superbubbles, and the largest one has linear scale is $\sim 500 - 1000 \text{ pc}$, due to about 3000 supernova explosions in $\sim 10^7 \text{ yr}$. The background density of their simulation is equivalent to that in the outer region of our simulations. The local ($< \text{kpc}$ scale) structure of

the ISM of our global simulations, where hot bubbles and cold filaments coexist, is also similar to the local, 2-D simulations of the ISM with a periodic boundary condition (Vázquez-Semadeni et al. 1995). In a conclusion, the past local models with supernova explosions, in which superbubble formation is reported, consistent with our global models with stellar energy feedback concerning the size of the superbubbles.

The cloud mass spectra of the model SF1 and SF2 are steeper than that of the model NSF (Fig. 8). In other words, the stellar energy input affects the evolution of molecular clouds. Vázquez-Semadeni, Balleseros-Paredes, & Rodriguez (1997) (hereafter VBR97) analyzed their 2-D hydromagnetic simulations and showed that the mass spectra have the form $dN_c/dM_c \propto M_c^{-1.44 \pm 0.1}$ (c.f. their Fig. 3 and our Fig. 8), and they reported that the mass spectra from observations are consistent with that from simulations in which the density field had been shaped by stellar activity. Note that our mass spectrum of the star formation models, the slope is shallower for smaller clouds ($M_c < 10^5 M_\odot$) than that for massive clouds ($dN_c/dM \propto M^{-2}$). Therefore our results might be consistent with the results of VBR97 (see also §3.2). However, direct comparison between these two results should not be straightforward, because there are number of differences between our simulations and theirs, on the numerical scheme (AUSM vs. pseudo spectral method), the boundary condition (global simulations vs. local periodic boundary), and the cooling curve especially for $T_g < 100$ K ($\Lambda \neq 0$ vs. $\Lambda = 0$). The maximum density contrast is about 5000 in their model, but it is about 2×10^6 in our model. This difference is caused probably due to the difference of the cooling curve for the cold gas, and also due to the numerical scheme. In their numerical method, they added a mass diffusion term to the continuity equation in order to smooth out the density gradients (see also Vázquez-Semadeni et al. 1995). This could affect the structure of shocks and dense gas, i.e, the cloud mass spectrum. The recipe for the stellar energy feedback are also different. VBR97 assumed that once a star is formed, then it remains fixed with respect to the numerical grid. In our models, the star particles are orbited in the self-gravitational potential of the gas and the external fixed potential. The last point, however, would not be important, if number of stars is large enough, or the ISM is fully turbulent. VBR97, on the other hand, include the magnetic field in their models. Therefore, again, one should be care-

ful to make direct comparison between results in the present paper and VBR97.

Our result implies that there are two mechanisms of cavity formation. One is the pure evacuation of gas from the low-density regions by the effect of the gravitational and thermal instabilities. Similar evacuation phenomena (Elmegreen 1994; Vázquez-Semadeni, Passot, & Pouquet 1996) are also observed in the simulations of the turbulent ISM without SNe (Passot, Vázquez-Semadeni, & Pouquet 1995). The other is the formation of cavities by the effect of SNe, and especially by the synchronized explosions of stars in OB associations. The two processes are essential to produce the whole structure of the ISM. The latter is necessary for hot ($T_g > 10^6$ K) component of the ISM. These two type of low-density regions are also observed in the two-dimensional, local simulations of the turbulent ISM with SNe by Gazol & Passot (1999).

As mentioned in §1, the origin of supergiant H I holes in galaxies has been controversial (see also Walter & Brinks 1999). If the observed kpc-scale holes and shells are caused by explosive phenomena only, one needs highly energetic events, like Gamma Ray Bursts (Loeb & Perna 1998). However, our numerical simulations give an alternative explanation about the origin of the large scale holes: the non-linear evolution of the multi-phase gas disk. In the multi-phase ISM, most of the gas mass is concentrated in the cold, dense clumps and filaments, but volume filling factor of such component is much smaller than that of hot, diffuse gas. The hot regions are surrounded by dense filaments as seen in Fig. 1 and Fig. 3. Therefore the multi-phase ISM in a quasi-steady state is naturally porous. Our results suggest that if the energy feedback from massive stars are not effective, kpc-scale inhomogeneity can be evolved in a disk in about several 10^8 yr. Dense filaments are changing in shape due to local random velocity field as well as the global shear, and often show kinematics features similar to those of “expanding shells” as seen in the position-velocity map (§3.3). We suspect that many supergiant holes and shells in dwarf galaxies do not have an explosion origin, but that supergiant shells far outside the disk plane can not be formed without explosive events.

The work presented here yields the model for the ISM in a LMC-type galaxy. Nevertheless there are couple of things that one should consider for constructing a complete numerical model of the LMC including the interaction with the Small Magellanic

Cloud, the optical bar, and non-uniform UV radiation field due to active star forming regions, such as the 30 Dor regions. The interactions with the SMC are important events for the star formation history in the LMC and the Magellanic Stream (Murai & Fujimoto 1980; Vallenari et al. 1996; Gardiner & Noguchi 1996). The off-center optical bar could also perturb the global structure of the ISM and star formation in the LMC (Gardiner, Turfus, & Putman 1998). However the H I mapping (Kim et al. 1998) does not show clear evidence of the stellar bar, namely off-set shocks which are often seen in barred galaxies. It would be interesting to investigate the effect of the off-center stellar bar in our model. This might contribute to the formation of the active star forming region, such as 30 Dor region.

In the present paper, we have not solved the vertical structure of the ISM. It is expected that the hot component behaves differently in three dimensions. The hot gas, which is above 10^6 K, cannot be confined in the disk plane (Rosen & Bregman 1995; Avillez 1999), and it would probably been blown out from the disk plane. The scale-height of the hot gas should be larger than the cold gas, and, as a result, the volume filling factor of the hot gas would be larger away from the disk plane. Thus the radiative cooling would be less effective in the hot gas, in three dimensions. This may affect interaction between cold and hot components, and the feedback process on the ISM. For example, it is more difficult to form the supergiant holes by SNe. In a subsequent paper, we will extend our method to three-dimensional modeling, and investigate these problems.

5. CONCLUSIONS

Using high resolution hydrodynamical simulations, we have computed that the global dynamics and structure of the multi-phase ISM in a LMC-type galaxy. Due to gravitational and thermal instability in the gas disk, clumpy fluctuations evolve, and then the clumps merge and form filamentary structure in the non-linear phase. Higher density clumps are formed in the filaments due to the gravitational instability, or collisions between the filaments. Our numerical model with the star formation allows us to provide the evolution of the blastwaves due to supernovae explosions in the rotating, inhomogeneous, multi-phase, and turbulent-like media. We find that the supernova rate in the model with stellar energy

feedback is typically of the order of 0.001 yr^{-1} during several hundred Myrs, but fluctuates rapidly (time scale ~ 10 Myr) by a factor of three or four. The model also shows that kpc-scale low density cavities seen in the observed H I map (Kim et al. 1998) are difficult to be formed under frequent supernovae, but SNe are necessary to form hot bubbles where the gaseous temperature is greater than 10^{6-7} K. Our result suggests that there are two possible causes of low density regions in the ISM. The kpc-scale inhomogeneity and arcs can be formed as a natural consequence of non-linear evolution of the multi-phase interstellar medium in a LMC-type galaxy. We find in the PV-diagram of the numerical models that filamentary structure in the non-star forming model, which are caused by the gravitational instability, has similar kinematics to the structure formed by SN explosions. The dense clouds are rotating, and about half of them show retrograde rotation against the sense of galactic rotation. Using the Monte Carlo radiative transfer code, we have computed H I and CO brightness temperature distributions, and compared them with those from the recent observations. The CO cloud mass spectrum in the model with stellar energy feedback is similar to the observed one (Fukui et al. 1999), but H I distribution function is well fitted by the model without SNe. Therefore we conclude that the small scale structure and dynamics of the ISM in the LMC is mainly affected by the stellar activities, but the gravitational instability significantly contributes to the global morphology and dynamics of the interstellar matter in a kpc-scale.

We are grateful to Colin Norman for stimulating discussions. We also thank E. Vázquez-Semadeni (the referee) for his fruitful comments and suggestions. Numerical computations were carried out on VPP300/16R at the Astronomical Data Analysis Center of the National Astronomical Observatory, Japan, VPP700 at the SUBARU observatory, Hawaii, and VPP500 at RIKEN, Japan. We would like to thank R. Ogasawara for his help at the SUBARU observatory. KW is supported in part by Grant-in-Aids for Scientific Research (no. 1113421) of Japanese the Ministry of Education, Culture, Sports and Science, and Foundation for Promotion of Astronomy, Japan. MS is supported by Hubble Fellowship grant HF-01101.01-97A, awarded by STScI.

Fig. 1.— Evolution of density and temperature distributions of a model without star formation and energy feedback (model “NSF”). The density and temperature are Log-scaled, and their units are $M_{\odot} \text{ pc}^{-2}$ and K, respectively. Time is shown at each panel in an unit, 10^8 yr . Note: Although the gray scale is assigned for $1000 - 0.01 M_{\odot} \text{ pc}^{-2}$ in this plot, the maximum density is much grater than $1000 M_{\odot} \text{ pc}^{-2}$ (see Fig. 2).

Fig. 2.— Evolution of the volume filling factor for four different phases, i.e. $T \leq 100 \text{ K}$ (filled circles), $100 < T \leq 9000 \text{ K}$ (open circles), $9000 < T < 10^5 \text{ K}$ (open diamonds), and $T \geq 10^5 \text{ K}$ (filled diamonds). The maximum density of the gas is also plotted (thin solid line).

Fig. 3.— Same as Fig. 1, but for a model with star formation and energy feedback (model “SF2”) at $t = 834 \text{ Myr}$.

Fig. 4.— Evolution of a total supernova rate in model SF2.

Fig. 5.— Star particles and density distribution at $t = 245 \text{ Myr}$ in model SF1.

Fig. 6.— Brightness temperature (T_B (K)) maps of H I (left) and CO (J=1-0) (right) computed from data of model NSF at $t = 800 \text{ Myr}$. The intensity of H I is Log-scaled.

Fig. 7.— Same as Fig. 6, but for model SF2 at $t = 834 \text{ Myr}$

Fig. 8.— (a) Mass spectrum of CO clouds for model NSF for three thresholds of the brightness temperature, $T_B = 30$ (solid line), 50 (dashed line), and 100 K (dotted line). The thick line shows $dN_c/dM_c \propto M^{-1.7}$. (b) Same as (a), but for model SF2.

Fig. 9.— Probability distribution function (pdf) of H I. Thick line shows pdf of model NSF ($N(T_B)$ is the number of cells for the brightness temperature, T_B , and N_0 is the total number of cells). The stars show the histogram from the H I synthesis observation, with $N^{1/2}$ error bars, which is normalized for $\log(T_B) = 2.8 \text{ K}$ of the model pdf.

Fig. 10.— Position-Velocity maps for (a) low density gas in model NSF, (b) high density gas in model NSF, and (c) low density gas in model SF1.

REFERENCES

Avillez, M. A. D. D. 1999, Stromlo Workshop on High-Velocity Clouds, eds. Gibson, B.K. & Putman, M.E., ASP Conference Series Vol. 166, p. 103, 103

Bakes, E. L. O. & Tielens, A. G. G. M. 1994, ApJ, 427, 822

Bania, T. M. & Lyon, J. G. 1980, ApJ, 239, 173

Chiang, W. -H. & Bregman, J. N. 1988, ApJ, 328, 427

Chiang, W. -H. & Prendergast, K. H. 1985, ApJ, 297, 507

Deul, E.R. & den Hartog, R.H. 1990, A&A, 229, 362

Elmegreen, B. G. 1994, ApJ, 433, 39

Feitzinger, V., Glassgold, A.E., Gerola, H., & Seiden, P.E. 1981, A&Ap, 98, 371

Fukui, Y., et al. 1999, PASJ, 51, 745

Gardiner, L. T. & Noguchi, M. 1996, MNRAS, 278, 191

Gardiner, L.T., Turfus, C., & Putman, M.E., 1998, ApJ, 507, L35

Gazol-Patino, A., & Passot, T., 1999, ApJ 518, 748

Gerritsen, J.P.E., Icke, V., 1997, A&Ap, 325, 972

Haberl, F. & Pietsch, W. 1999, A&AS, 139, 277

Hockney, R. W., & Eastwood, J. W. 1981, Computer Simulation Using Particles (New York : McGraw Hill)

Ikeuchi, S., Habe, A., & Tanaka, Y.D. 1984, MNRAS, 207, 909

Kim, S., Staveley-Smith, L., Dopita, M.A., Freeman, K.C., Sault, R.J., Kesteven, M.J., & McConnell, D., 1998, ApJ, 503, 674

Kim, S., Dopita, M.A., Staveley-Smith, L., Bessell, M. 1999, AJ, 118, 2797.

Kim, S. & Chu, Y.-H. 2000, in preparation.

Korpi, M. J., Brandenburg, A., Shukurov, A. & Tuominen, I. 1999, A&A, 350, 230

Liou, M., Steffen, C. 1993, J.Comp.Phys., 107, 23

Loeb, A. & Perna, R. 1998, ApJ, 503, L35

Leitherer, C., Robert, C. & Drissen, L. 1992, ApJ, 401, 596

McKee, C.F. & Ostriker, J.P. 1977, ApJ, 218, 148

Murai, T. & Fujimoto, M. 1980, PASJ, 32, 581

Norman, C.A., & Ikeuchi, S. 1989, ApJ, 345, 372

Oey, M. S. 1996, ApJ, 467, 666

Oey, M. S. & Clarke, C. J. 1997, MNRAS, 289, 570

Passot, T., Vázquez-Semadeni, E., & Pouquet, A. 1995, ApJ, 455, 536

Puche, D. , Westpfahl, D. , Brinks, E. & Roy, J. -R. 1992, AJ, 103, 1841

Rhode, K.L., Salzer, J.J., Westpfahl, D.J., & Radice, L.A. 1999, AJ in press (astro-ph/9904065)

Rosen, A., Bregman, J.N., 1995, ApJ, 440, 634

Scalo, J., Chappell, D., 1999, ApJ 510, 258

Seiden, P. E. & Gerola, H. 1982, Fundamentals of Cosmic Physics, 7, 241

Shore, S. N. & Ferrini, F. 1995, Fundamentals of Cosmic Physics, 16, 1

Spaans, M. , Tielens, A. G. G. M., Van Dishoeck, E. F. & Bakes, E. L. O. 1994, ApJ, 437, 270

Spaans, M. 1996, A&A, 307, 271

Spaans, M., Norman C., 1997, ApJ, 483, 87

Spaans, M. & Van Dishoeck, E. F. 1997, A&A, 323, 953

Spitzer, L. 1978, John Wiley & Sons, Inc., New York, p. 139

Stanimirovic, S., Staveley-Smith, L., Dickey, J. M., Sault, R. J. & Snowden, S. L. 1999, MNRAS, 302, 417

Stone, J., & Norman, M.N. 1992, APJS, 80, 753

Staveley-Smith, L., Sault, R. J., Hatzidimitriou, D., Kesteven, M. J. & McConnell, D. 1997, MNRAS, 289, 225

Tenorio-Tagle, G. 1988, ARA&A, 26, 145

Vázquez-Semadeni, E., Passot, T. & Pouquet, A. 1995, ApJ, 441, 702

Vázquez-Semadeni, E., Passot, T. & Pouquet, A. 1996, ApJ, 473, 881

Vázquez-Semadeni, E., Ballesteros-Paredes, J., & Rodriguez, L.F., 1997, ApJ, 474, 292

van der Hulst, J.M. 1996, in ASP Conf. Ser. Vol. 106: The Minnesota Lectures on Extragalactic Neutral Hydrogen, ed. E.D. Skillman (ASP: San Francisco), 47

Van Dishoeck, E. F. & Black, J. H. 1988, ApJ, 334, 771

Vallenari, A., Chiosi, C., Bertelli, G. & Ortolani, S. 1996, A&A, 309, 358

Wada, K., & Norman, C., 1999, ApJ, 516, L13

Walter, F. & Brinks, E. 1999, AJ, 118, 273

Woodward, P. R., & Colella, P. 1984, J.Comp.Phys., 54, 115

This figure "Fig1.gif" is available in "gif" format from:

<http://arxiv.org/ps/astro-ph/0005330v1>

This figure "Fig3.gif" is available in "gif" format from:

<http://arxiv.org/ps/astro-ph/0005330v1>

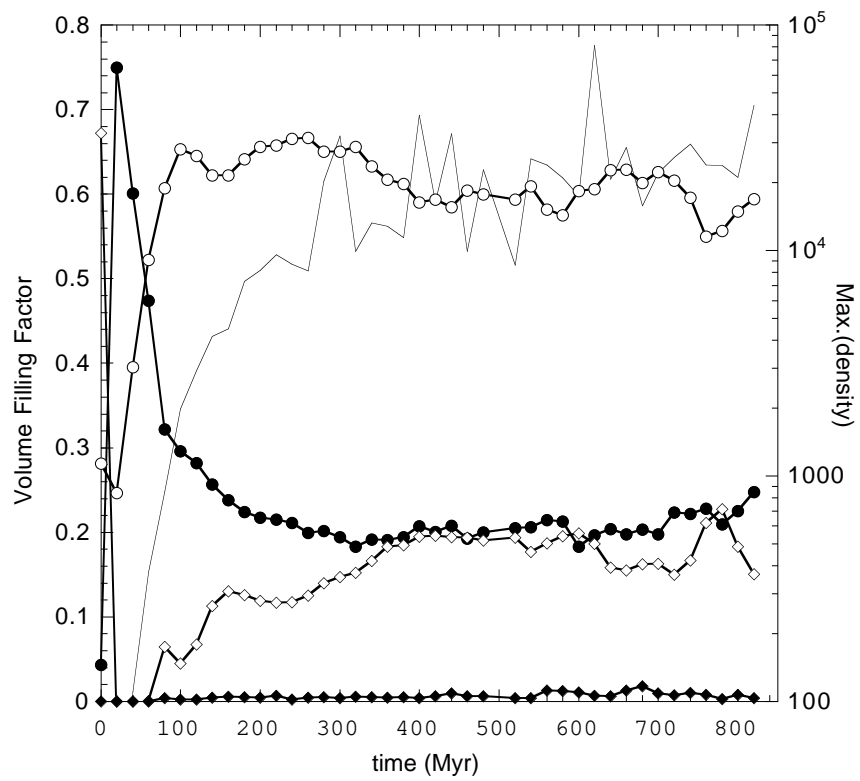


Fig. 2

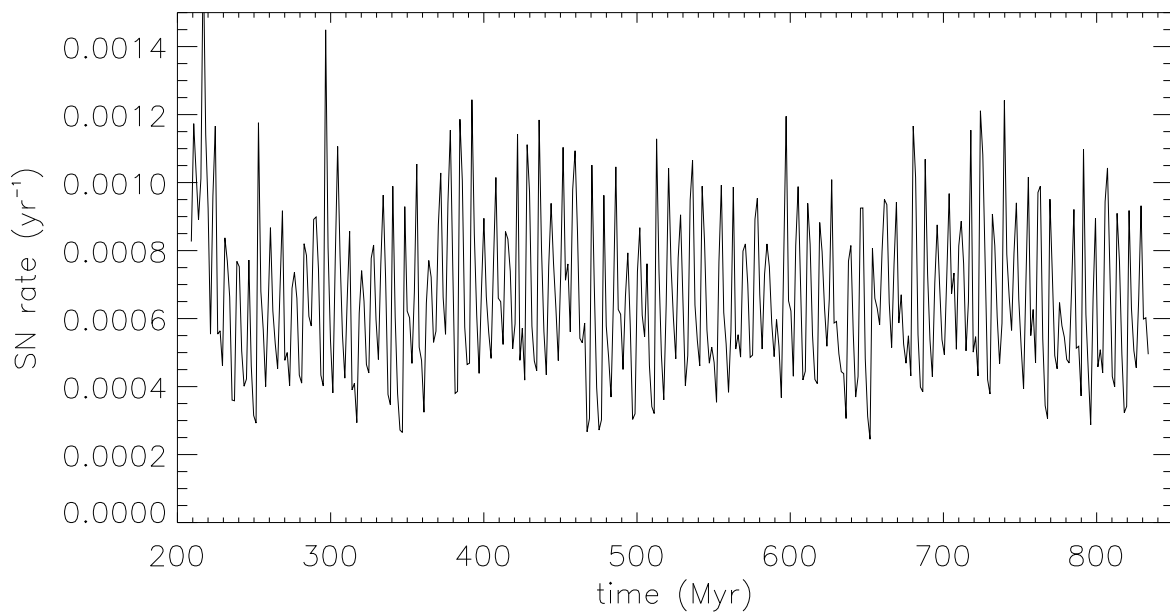


Fig. 4

This figure "Fig5.gif" is available in "gif" format from:

<http://arxiv.org/ps/astro-ph/0005330v1>

This figure "Fig6.gif" is available in "gif" format from:

<http://arxiv.org/ps/astro-ph/0005330v1>

This figure "Fig7.gif" is available in "gif" format from:

<http://arxiv.org/ps/astro-ph/0005330v1>

Fig. 8(a)

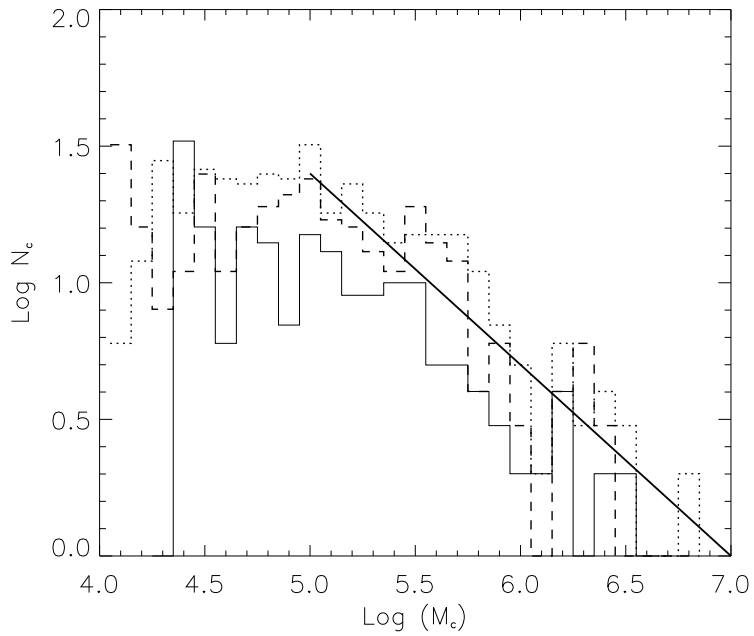


Fig.8(b)

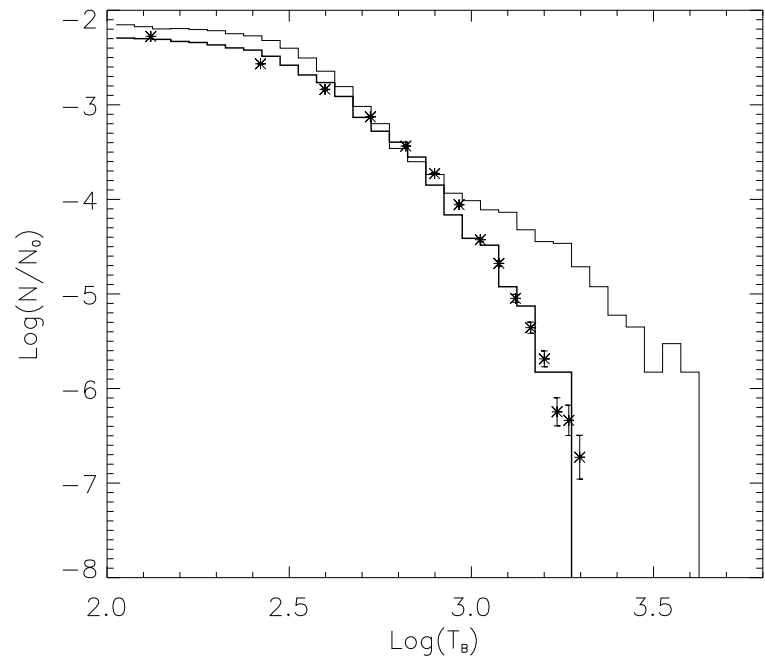
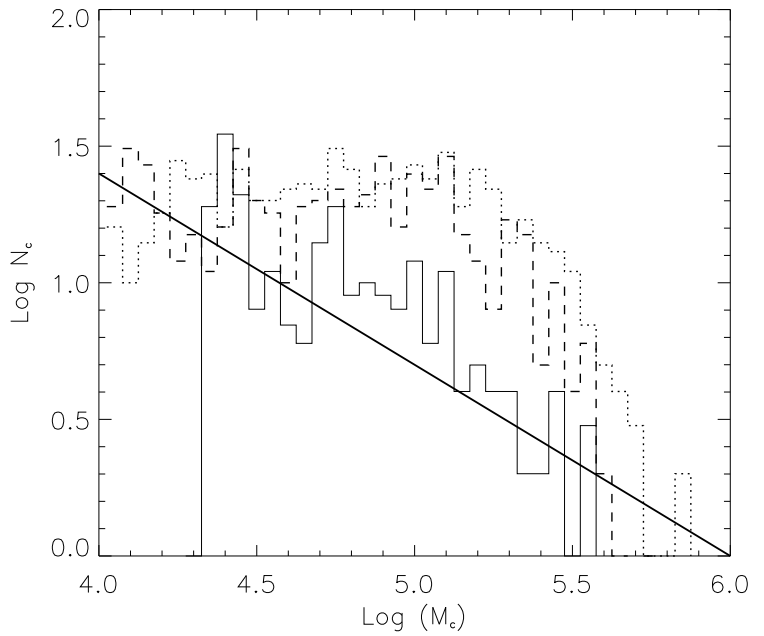


Fig. 9

This figure "Fig10.gif" is available in "gif" format from:

<http://arxiv.org/ps/astro-ph/0005330v1>